Robust estimate of dynamo thresholds in the von Kármán sodium experiment using the extreme value theory

2014 New J. Phys. 16 083001

(http://iopscience.iop.org/1367-2630/16/8/083001)

New Journal of Physics
The open access journal at the forefront of physics
Deutsche Physikalische Gesellschaft DPG | IOP Institute of Physics

Robust estimate of dynamo thresholds in the von Kármán sodium experiment using the extreme value theory

Davide Faranda[1], Mickaël Bourgoin[2,3], Sophie Miralles[2], Philippe Odier[2], Jean-François Pinton[2], Nicolas Plihon[2], Francois Daviaud[1] and Bérengère Dubrulle[1]

[1] Laboratoire SPHYNX, Service de Physique de l'Etat Condensé, DSM, CEA Saclay, CNRS URA 2464, 91191 Gif-sur-Yvette, France
[2] Laboratoire de Physique, École Normale Supérieure de Lyon, CNRS & Université de Lyon, 46 allée d'Italie, 69364 Lyon Cedex 07, France
[3] Laboratoire des Écoulements Géophysiques et Industriels, CNRS & Université Joseph Fourier, BP 53, 38041 Grenoble Cedex 9, France
E-mail: davide.faranda@cea.fr

Received 18 February 2014, revised 7 May 2014
Accepted for publication 18 June 2014
Published 1 August 2014

New Journal of Physics **16** (2014) 083001
doi:10.1088/1367-2630/16/8/083001

Abstract

We apply a new threshold detection method based on the extreme value theory (EVT) to the von Kármán sodium (VKS) experiment data. The VKS experiment is a successful attempt to get a dynamo magnetic field in a laboratory liquid-metal experiment. We first show that the dynamo threshold is associated with a change of the probability density function of the extreme values of the magnetic field. This method does not require the measurement of response functions from applied external perturbations and thus provides a simple threshold estimate. We apply our method to different configurations in the VKS experiment, showing that it yields a robust indication of the dynamo threshold as well as evidence of hysteretic behaviors. Moreover, for the experimental configurations in which a dynamo transition is not observed, the method provides a way to extrapolate an interval of possible threshold values.

Keywords: extreme value theory, turbulent dynamo, early warnings, critical transitions

It is generally accepted that the planetary magnetic field is generated by dynamo action, an instability mechanism inside the liquid conducting fluid of the planetary core. There is, however, presently no general theory providing an estimate for the corresponding dynamo threshold, except in some particular cases [1–3]. The main difficulties in computing the threshold derive from the turbulent nature of the flow, which makes the dynamo action akin to a problem of instability in the presence of a multiplicative noise [4]. As more and more data from experiments are available [5–7], the possibility of devising precise, almost automated methods for dynamo threshold detection would be welcome. The statistical approach to this question traditionally involves so-called indicators of criticality [8]. Some of these indicators are based on modifications of the auto-correlation properties of specific observables when parameters controlling the system approach some critical value. Others are based on the fact that an increase of the variance and the skewness is observed when moving towards tipping points [9]. Still other approaches are based on the definition of ad hoc susceptibility functions or critical exponents [10–12]. In [12, 13], the decay of external applied magnetic field pulses is studied, and the transition is detected through the divergence of the decay times near the dynamo threshold. Although interesting for controlled laboratory applications, this approach cannot be extended to problems involving planetary scales. In this paper, we suggest that the statistical approach based on the extreme value theory (EVT) proposed in [14] could provide a robust determination of the threshold even in the presence of turbulence. The main advantage of the present method is that it yields to a precise and unique determination of the threshold as the location of zero crossing of a statistical parameter κ. It therefore works even in the case of the imperfect bifurcation that usually occurs in experimental dynamo due to the ambient magnetic field (mainly the Earth field), residual magnetization of the disks, and other magnetic perturbations of the setup. To illustrate the possibilities of the method, we analyse data from the VKS experiment consisting of a von Kármán swirling flow of liquid sodium. In this experiment, turbulent effects are roughly of the same order as the mean flow. The control parameter of the system is the magnetic Reynolds number Rm, which is proportional to the driving impellers, rotation frequency F. Several dynamo and non dynamo configurations have been obtained by changing the material of the impellers and of the cylinder [12, 15] and by varying the impellers, rotation frequency. This versatility allows for reproducing a spectrum of magnetic field dynamics that can be observed for the planetary magnetic fields such as reversal [5], bistability [11, 16], or localization [17]. Applying our method to several different configurations, we show in the present article that it provides a robust indication of the dynamo threshold as well as evidence of hysteretic behaviors.

1. Method

We use the statistical approach based on the EVT proposed in [14] as a criterion allowing the determination of the dynamo threshold. We briefly recall the basic intuition beyond the method referring to [14] for further discussions. Classical EVT states that, under general assumptions, the statistics of *maxima* $M_m = \max\{X_0, X_1, ..., X_{m-1}\}$ of independent and identically distributed variables $X_0, X_1, ..., X_{m-1}$, with cumulative distribution function (cdf)

$F(x)$ in the form:

$$F(x) = P\left\{a_m\left(M_m - b_m\right) \leqslant x\right\},$$

where a_m and b_m are normalizing sequences, asymptotically obeys a generalized extreme value (GEV) distribution with cumulative distribution function:

$$F_G(x;\, \mu,\, \sigma,\, \kappa) = \exp\left\{ -\left[1 + \kappa\left(\frac{x-\mu}{\sigma}\right)\right]^{-1/\kappa}\right\} \tag{1}$$

with $1 + \kappa(x - \mu)/\sigma > 0$. The *location parameter* $\mu \in \mathbb{R}$ and the *scale parameter* $\sigma > 0$ in equation (1) account for the normalization of the data, avoiding the recourse to scaling constants a_m and b_m [18].

The sign of κ discriminates the kind of tail decay of the parent distribution: When $\kappa = 0$, the distribution is of Gumbel type (type 1). This is the asymptotic extreme value law (EVL) to be expected when the parent distribution shows an exponentially decaying tail. The Fréchet distribution (type 2), with $\kappa > 0$, is instead observed when the parent distribution possess a fat tail decaying as a power law. Eventually, the Weibull distribution (type 3), with $\kappa < 0$, corresponds to a parent distribution having a finite upper endpoint. When properties of *maxima* and *minima* are of interest, respectively corresponding to the exploration of the right or left tails of the parent distribution, they can be treated on an equal footing by considering the *minima* as *maxima* of the variables after sign reversal [19]. Physical observables have generally bounded fluctuations, and their extremes follow Weibull distributions [20, 21]. Gaussian fluctuations (featuring Brownian motion of microscopic degrees of freedom) would yield the formal possibility of infinite extremes and thus Gumbel distributions, but the convergence towards this law is logarithmically slow [22] so that a Weibull law is observed in these cases as well.

The interest of the EVL statistics in bifurcation detection relies on the change of the nature of the fluctuations of a given system, when going from a situation with one stable attractor to a situation with two competing attractors, with a jump between the two allowed either under the effect of external noise or due to internal chaotic fluctuations. In such a case, two time scales are present: a short one related to transitive dynamics within an attracting component and a long one corresponding to intermittent jumps from one to the other component. The fluctuations and their extreme are then of a different nature over the two time scales: over the long time scale, some extremes correspond to noisy excursions directed toward the saddle-state and gain a *global* status, as they can trigger jumps from one to the other component. The probability increases as the observable visits correspond to 'anomalous' values associated to these global extremes during a time series of length s, and the tail of the parent distribution becomes large. Through the bifurcation, we are thus in a situation where the parent distribution goes from bounded fluctuations (with extreme converging to a Weibull law) to fluctuations with fat tails (with extreme converging to a Fréchet distribution). The shape parameter κ then changes through the bifurcation from $\kappa < 0$ to $\kappa > 0$, which enables a precise definition of the threshold as the value at which the zero crossing of κ happens. Physical observables will display deviations of greater amplitude in the direction of the state the system is doomed to tumble—that is, the basin of attraction observed after the transition—than in, the opposite direction; therefore, one expects to observe this switching either in the *maxima* or in the *minima*.

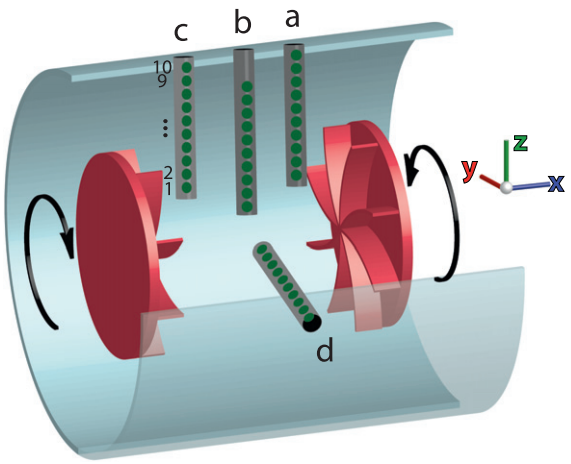

Figure 1. Experimental setup showing the location of the Hall probes, where x is the axial coordinate directed from impeller 1 to impeller 2.

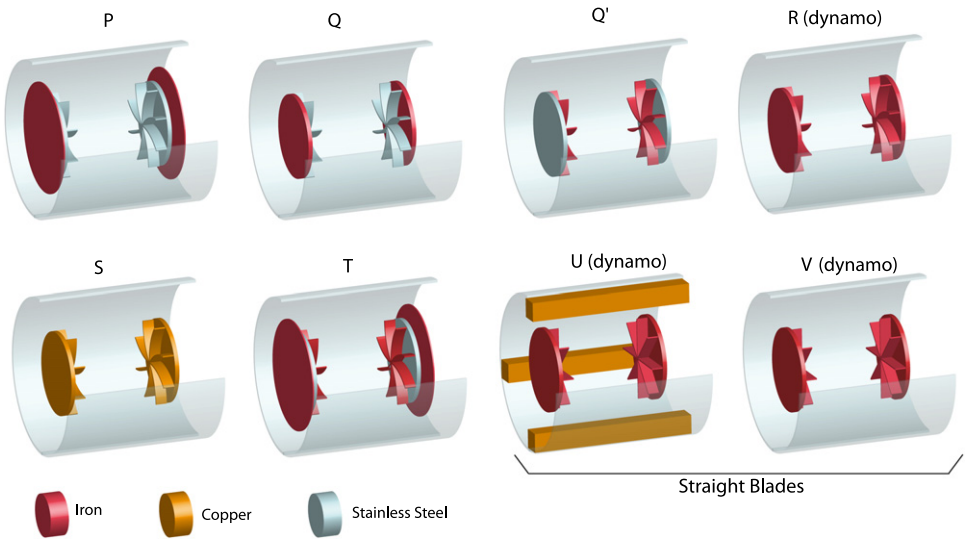

Figure 2. Schematic representation of the studied VKS configurations. Gray stands for stainless steel, yellow for copper, and red for soft iron.

2. Experimental setup

Here we focus on the VKS experiment, consisting of a von Kármán swirling flow of liquid sodium. The dynamo is generated in a cylinder of radius $R_0 = 289$ mm by the motion of two coaxial discs of radius $R_{imp} = 154.5$ mm, counter-rotating at a frequency F. We define the magnetic Reynolds number as: $Rm = 2\pi\mu_0\sigma R_{imp}R_0F$, where $\sigma = 9.6 \times 10^6\ \Omega \cdot \mathrm{m}^{-1}$ is the sodium electrical conductivity and μ_0 the permeability of vacuum. In the sequel, we use data from the eight configurations obtained by changing the material of the impellers and of the cylinder as shown in figure 2 and described in [12]. Magnetic fields are recorded using four arrays of 10 three-axis Hall effect sensors inserted in radial shafts, as shown in figure 1. Two arrays are inserted in the mid-plane of the vessel within long probe shafts (labeled b and d in

figure 1); the other two are inserted closer to the impellers within shorter probe shafts (labeled a and c in figure 1). These magnetic field at the sensors are recorded at a rate of 2000 Hz, with accuracy ± 0.1 G. Overall, the probes provide measurements of the three components of the magnetic field $\vec{B}(t)$ as a function of time t.

3. Application to VKS data

We present the results for the detection of the dynamo threshold Rm^* by using as observable the modulus of the magnetic field $|\vec{B}(t)|$ measured by the 40 different detectors (Hall probes).

The method can be described as follows. First of all, the extremes of the magnetic field are extracted by using the so called *block maxima approach*, which consists in dividing the series $|\vec{B}(t)|$, $t = 1, 2, ..., s$ into n bins, each containing m observations ($s = nm$) and thus selecting the maximum (minimum) M_j in each bin. The series of M_j, $j = 1, ..., n$ is then fitted to the GEV distribution via the L-moment procedure described in [23]. In order to sample proper extreme values, one must consider a bin length longer than the correlation time τ. For each of the sensors we have computed τ as the first zero of the autocorrelation function, finding that 0.42 s $<\tau<$ 1 s lags, depending on the cases considered. This value is similar to the magnetic diffusion time found in [24]. By choosing a bin duration longer than 1 s (or, equivalently, a number of samples m in each bin larger than 2000) and repeating the fit until the shape parameter κ is not changing appreciably, one can establish the convergence to the GEV model [18]. In our experiments we found that reliable estimates can be generally obtained for $m > 4000$. Being the length of each series $10^5 < s < 3 \cdot 10^5$, for any choice of $m > 4000$, no more than $n = 100$ *maxima* can be extracted. Such a value of n is one order of magnitude smaller than the one prescribed in [25, 26] for avoiding biased fits to the GEV model. In order to overcome this problem, we have grouped sensors located at the same radial position. The sensors of the four arrays of Hall effect sensors are not installed at the same radial distance (see figure 1 for a visual explanation). However, an effective radial grouping can be obtained by adding to the n extremes of the sensor a_l the ones of b_{l+2}, c_l and d_{l+2}, $l = 1, ..., 8$, thus obtaining eight different series with a sufficient number of *maxima* to perform the fit. The choice of grouping the sensors by their radial location is justified by checking that the shape of the distribution, which enters in the computation of the shape parameter κ, does not change substantially for sensors located at the same radial position. In order to do so, we have computed the skewness and the kurtosis for the time series of the magnetic field, finding small variations for sensors located at the same radial position. By analyzing the cross-correlation function of different sensors, we also checked that the *maxima* extracted by combining the series are independent. For example, for sensors a and b, the cross-correlation function is defined as:

$$\tilde{\tau}_{M(a),M(b)}(h) = \frac{1}{n}\sum_{i=1}^{n-h}\left(M_j(a) - \left\langle M_j(a)\right\rangle_j\right)\left(M_{j+h}(b) - \left\langle M_j(b)\right\rangle_j\right).$$

Here, the notation $\langle \cdot \rangle_j$ indicates the expectation value taken over the j index. The results of this analysis are shown in figure 3 for *maxima* in the case $Rm \simeq 33.8$, sensors index 5, in the R configuration. The plots on the left refer to $m = 1000$, the ones on the right to $m = 4000$. From top to bottom we represent $\tilde{\tau}(h)$ respectively for $h = 0$, $h = +5$, and $h = -5$. The case $h = 0$ corresponds to sensors located at the same radial position, which we grouped in our study. One can observe that although the correlation is non-zero, it is relatively small (about 0.5 for

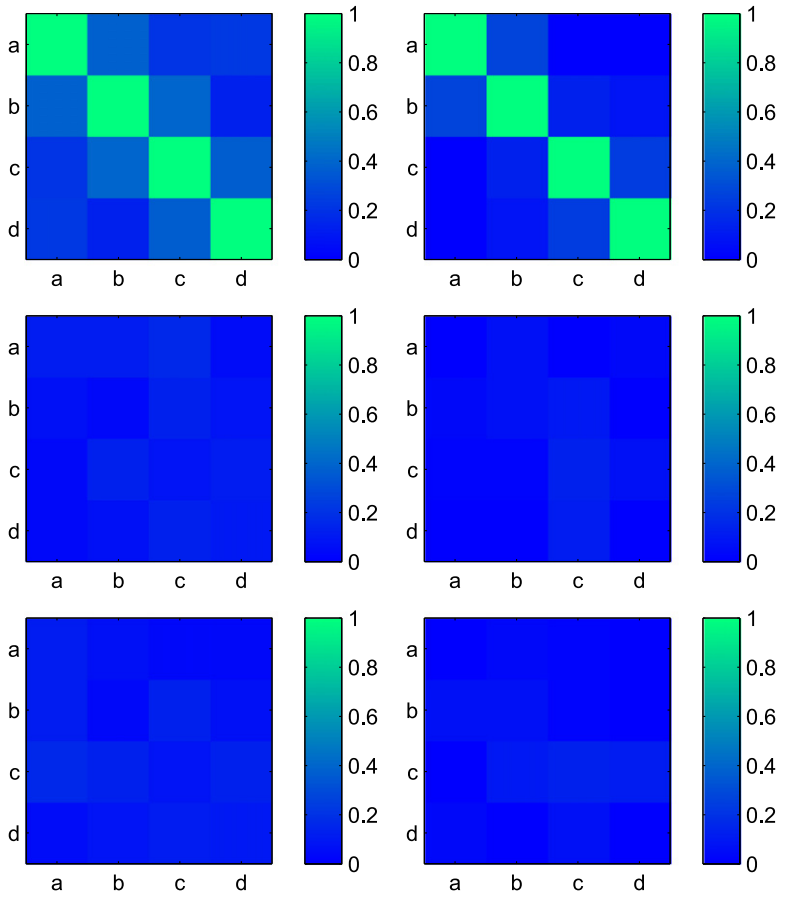

Figure 3. Cross correlation $\tilde{\tau}_{M(\lambda),M(\mu)}(h)$ for $m = 1000$ (left panels) and $m = 4000$ (right panels) $\lambda = \{a, b, c, d\}$, $\mu = \{a, b, c, d\}$. From top to bottom panels: $h = 0$, $h = 5$, $h = -5$. R configuration, $Rm \simeq 33.8$.

neighboring probes and smaller than 0.2 for non-neighbouring probes), which validates our grouping of the sensors to increase our statistics. In addition, for sensors located at different radial positions, the decorrelation is total (see the example at $h = \pm 5$ in figure 3; note that the decorrelation already starts at $h = \pm 1$). This indicates that the different series we show are totally independent.

Due to the different size of the fluctuations, extremes have been renormalized using the following, rather standard, definition:

$$\tilde{M}_j(a_l) = \frac{\left(M_j, a_l - \left\langle M(a_l)\right\rangle_j\right)}{\sqrt{\left\langle M_j(a_l) - \left\langle M(a_l)\right\rangle_j\right\rangle_j}}.$$

The same normalization applies for the sensors b, c, d. There are less trivial ways of normalizing the extremes; e.g., by choosing other location indicators than the expected value, such as the median or the mode (the most probable value). We thus replaced the mean with such indicators and checked that the results do not change in an appreciable way.

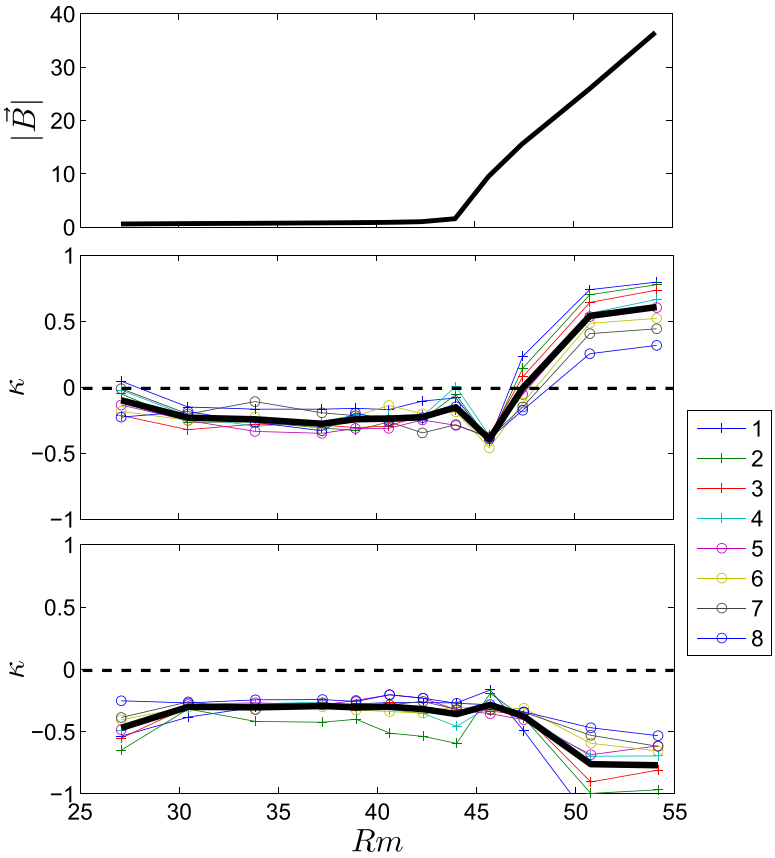

Figure 4. Upper panel: bifurcation in terms of the magnetic field averaged over all the sensors. Central panel: shape parameters for the *maxima* versus magnetic Reynolds number for the eight groups of sensors (each in a different color), $\langle k \rangle_l$ (thick black line), and Gumbel law $\kappa = 0$ (dashed line) in the R configuration. Lower panel: same as the central panel but for the *minima*.

4. Results

We begin the analysis by computing the dynamo threshold Rm^* in the experiments performed with the configuration R, featuring soft iron impellers. This configuration produces a well-documented stationary dynamo at $Rm \approx 44$, thereby providing a fair test of our method [27]. In the run we analyse, the Reynolds magnetic number is increased monotonically from $Rm \simeq 26$ up to $Rm \simeq 54$. By monitoring the value of $|\vec{B}|$ as a function of Rm, represented in the upper panel of figure 4, one observes a sudden increase of the magnetic field amplitude around the value $Rm \approx 44$, leading to a first definition of the threshold parameter as $Rm^* = 44$.

The observation of variations of $|\vec{B}|$ provides interesting information about the detection of the threshold through the EVL method. Indeed, since beyond the dynamo threshold Rm^* the values of $|\vec{B}|$ are significantly higher, we expect to detect the transition by the change of sign of the *maxima* distribution, whereas the *minima* shape parameter should remain negative even across the transition. Results are shown in figure 4 for the shape parameter of the *maxima* (central panel) and of the *minima* (lower panel). Each color represents the curve of κ obtained by grouping the sensors located at the same radial position, whereas the thick lines respectively

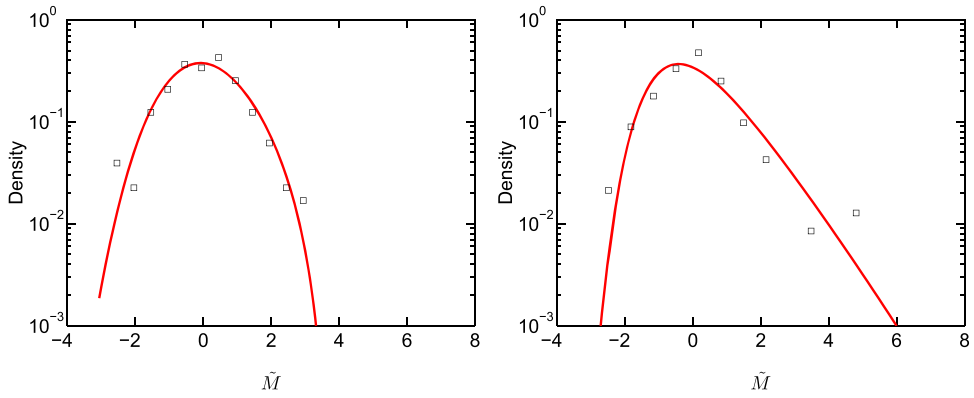

Figure 5. Two histograms for the normalized *maxima* $\tilde{M}$ of the sensors 6 (black markers) and correspondent fits to the GEV distribution (red lines). Left: $Rm \simeq 27$ the *maxima* are bounded: $\kappa = -0.21$. Right: $Rm \simeq 48$, some *maxima* are detached with respect to the bulk statistics. These events trigger the transition of κ towards positive values: $\kappa = +0.01$.

represent an average over l (solid black line) and the Gumbel law (dashed black line). When Rm is approaching 47, the average shape parameter for the distribution of *maxima* first decreases then increases and changes sign at $Rm = 47$, whereas for the *minima* it remains negative. We therefore set the threshold value $Rm^* \simeq 47$. The decrease before the change of sign might be a signature of earth-field expulsion before dynamo onset. The change of sign, characteristic of dynamo onset, is associated with a change in the nature of distribution of *maxima* of the magnetic field, as expected from EVL theory. Indeed, we have plotted in figure 5 two histograms for the *maxima* distribution: one for a value of Rm far from the transition (left plot) and one for Rm close to the bifurcation (right plot). Whereas in the first case the distribution of *maxima* is bounded above, in the second case the largest values of $\tilde{M}$ will eventually trigger the transition and are responsible for the change of sign of κ. One may note in figure 4 that, contrary to the transition presented in [14], here there is an evident effect also on the *minima* shape parameter, which tends to more negative values for $Rm > Rm^*$.

We see from this example that the threshold determination using the EVL provides a value about 7 percent higher than the value based on $|\vec{B}|$. We may note that, due to the ferromagnetic nature of the disk material, the dynamo bifurcation is naturally imperfect. This results in a smoothing of the variation of $|\vec{B}|$ near the threshold that may lead to an underestimation of the perfect threshold. In contrast, the threshold computed using the EVL is obtained via topological change of the attracting basins and may point to a value that is closer to the perfect threshold. To quantify this, we may first resort to a statistical analysis of our results, using the different sensor locations. By analyzing the results obtained at low frequencies of rotations, the fit for each group of sensors returns a shape parameter statistically dispersed around the average, with no radial dependence. On the contrary, for $Rm > Rm^*$, the shape parameter crosses zero for increasing values of Rm as the radial location of the sensors increases. This effect is even more pronounced for sensors outside the flow (i.e., sensor 9 and 10 of probes a and c, not shown in figure 4, since at these radial locations only two sensors were available instead of four). This means that the threshold detection based only on external sensors is likely to overestimate the threshold. This has, of course, great implications for the detection of the threshold of magnetic fields from planetary observation, as we are likely to observe only an equivalent of the outer

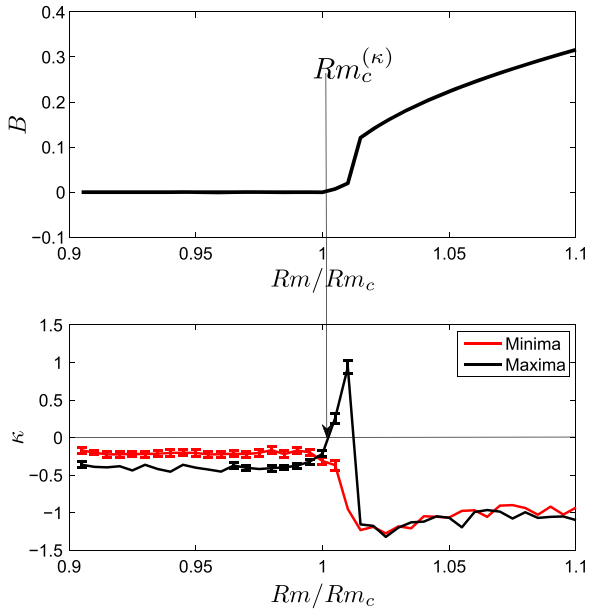

Figure 6. Upper panel: average magnetic field $|B|$ for the model introduced in equation (2). Lower panel: Shape parameter κ for the *maxima* of the *minima* of B, as obtained by integrating equation (2) with an Euler scheme at $\xi = \psi = 0.01$, $dt = 1$, and $B(0) = 0.1$ as initial condition.

sensors. Nevertheless, this analysis confirms *a posteriori* the reasonableness of grouping the sensors at the same radial position and provides an error bar on our threshold determination.

To estimate the error bar of the threshold with respect to the perfect threshold, we may follow [14] and apply the technique on a simple theoretical model that captures the main features of dynamo transition. As discussed in [4], the dynamo transition in a turbulent medium may be seen as a bifurcation with a multiplicative noise. To further model the experimental noise and fluctuations caused by induction of the magnetic field present in the building where the experiment is performed, we further introduce an additive noise term and consider the following simple stochastic model:

$$dB/dt = (Rm + \epsilon\xi(t))B - B^3 + \eta\psi(t), \tag{2}$$

where ξ and ψ are normal identically distributed variables, ϵ and η are respectively the variances of the multiplicative and the additive noise, and Rm is the control parameter such that instabilities appear for $Rm > 1$. We then perform the same analysis as for the experimental data and analyse time series, each taken at a different Rm with $0.95 < Rm < 1.05$, consisting of 10^6 observations. Other parameters are fixed as: $\xi = \psi = 0.01$, $dt = 1$, and $B(0) = 0.1$ as initial condition. Results are robust with respect to changes in the parameters and initial conditions, as we tested. For each of the Reynolds magnetic numbers Rm, the shape parameter κ is represented in figure 6. As for the real dynamo experiment, the shape parameter for the *maxima* changes sign from negative to positive at $Rm_c^{(\kappa)} = 1.005$, resulting in an overestimation of the threshold by a factor 5 per thousand. For all the Rm considered, κ for the *minima* remains negative. For higher values of ψ and ξ, we get even better precision for the threshold estimate, as larger fluctuations increase the probability of observing extremes directed towards the dynamo attracting state. Including imperfection to the transition does not change this conclusion. This

Table 1. Dynamo threshold for various configuration in the VKS experiment, obtained through various techniques. $Rm_{|\vec{B}|}$: from the increase of the magnetic field amplitude $|\vec{B}|$ [10, 11]; Rm_f^* and Rm_b^*: forward and backward threshold obtained from the extreme value technique, with zero crossing detection (this paper); Rm^e: from the extreme value technique, with cubic extrapolation to detect zero crossing (this paper); Rm^d: from decay time divergency extrapolation [12]; Rm^i: from induction increase extrapolation.

Run	$Rm_{\|\vec{B}\|}$	Rm_f^*	Rm_b^*	Rm^e	Rm^d	Rm^i
P	—	—	—	—	—	—
Q	—	—	—	—	—	200
Q'	—	—	—	85 ± 10	350	125
R	44	46	37	—	51	56
S	—	—	—	150 ± 25	—	—
T	—	—	—	100 ± 25	250	205
U	70	75	66	—	58	100
V	66	67	45	—	71	93

simple model therefore indicates that the threshold determination via the EVL is robust and provides the critical Rm with good precision. Based on this, we conclude that the critical magnetic Reynolds number for the dynamo in this VKS experiment is around $Rm^* \simeq 47$ and that the lower value $Rm_c^* = 44$ is probably an underestimate due to imperfection effects. Note that in the theoretical model with multiplicative and additive noise, κ again attains negative values for $Rm > 1.02$ as a consequence of the solution falling in a new attraction basin with bounded fluctuations. In the experiment, we do not observe such an effect, since κ remains positive within the explored range of Rm. A first explanation could be that the range of Rm explored is not wide enough; therefore we still have not yet reached the new attraction state. Another more likely explanation is that the one-dimensional model fails to capture the complexity of the dynamo attractor that may be multidimensional.

Hysteresis has been previously reported in the VKS experiment [10, 27] and was also observed in the R configuration under scrutiny here: in order to shut down the dynamo, one has to decrease the magnetic Reynolds number to values smaller than Rm^*. This is presumably an effect of the residual magnetization of the iron impellers. This hysteresis is a good test for further validation of the results obtained via the extreme value based technique, since the curve of the shape parameter should be able to detect some hysteretic behavior. If we redefine the dynamo activation threshold found in the previous analysis as $Rm_f^* = 47$, f indicating the first passage in the forward direction of the experiment, we expect to find a dynamo deactivation threshold $Rm_b^* < Rm_f^*$, b indicating the backward experiment obtained by decreasing Rm from $Rm \simeq 55$ to $Rm = 30$. We have then analysed a run in which the magnetic Reynolds number is first increased monotonically from $Rm \simeq 26$ up to $Rm \simeq 54$, then decreased monotonically from $Rm \simeq 54$ up to $Rm \simeq 26$. The results shown in figure 7 for the *maxima* average shape parameter $\langle \kappa \rangle_l$ $l = 1, \ldots 8$ clearly indicate the presence of a hysteresis cycle in agreement with expectation. We have already commented on the forward part of the experiment repeated in figure 7 for clarity and represented by the right arrows. When the frequency is instead decreased, a Fréchet EVL is observed until $Rm_b^* \simeq 37 < Rm_f^*$. At this value, the shape parameter crosses the Gumbel law and approaches again the Weibull distribution of the *maxima*. Note also that the shape parameter for the *minima* (not shown here) remains always negative even in the backward transition, as expected by the theory described so far.

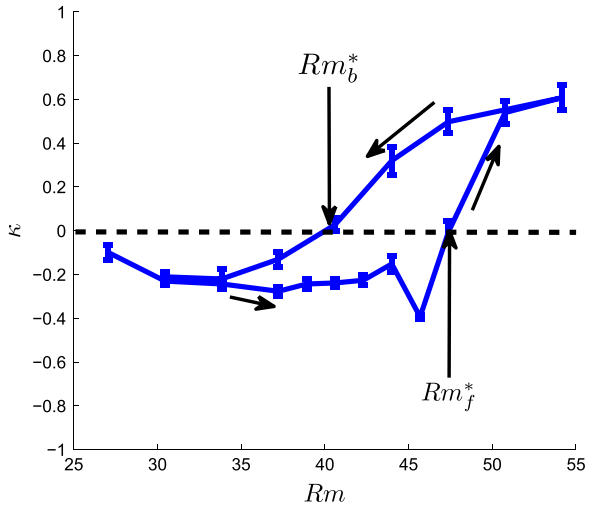

Figure 7. Diagram of $\langle\kappa\rangle_l$ (blue line) and Gumbel law $\kappa = 0$ (dashed black line) versus magnetic Reynolds number in the R configuration. The arrows indicate the direction of variation of Rm in the experiment.

The same analysis has been carried out for all the configurations shown in figure 1. The corresponding Rm_f^* and Rm_b^* are reported in table 1. For comparison, we have included in the table values, estimated via three other techniques: from the increase of the magnetic field amplitude $|\vec{B}|$ (denoted $Rm_{|\vec{B}|}$) [10, 11], from decay time divergence Rm^d[12], and via induction Rm^i [12]. The value of the shape parameter remains negative for both the *maxima* and the *minima* in the configurations P, Q, Q', S, T where dynamos have not been observed, whereas the method is able to detect the dynamo and the hysteretic behavior for the U and V setup. These results are in agreement with [12]. For the configurations for which the dynamo (run P, Q, Q', S, T) is not observed within the range of accessible Rm, it is interesting to follow [12] and try to estimate the possible dynamo threshold by extrapolation techniques. Indeed, in the Q', S, and T, we observed that the values of κ increase monotonically for at least the three consecutive highest Rm. An example is shown for the Q' configuration in figure 8. An extrapolate threshold value Rm^e can then be found by applying a polynomial fit of the $\langle\kappa\rangle_l$ curve and detecting the location of the zero crossing. Of course, as seen in figure 8, the value of Rm^e depends on the order of the polynomial fit; e.g., the value of Rm^e obtained by a linear and a quadratic fit is larger than what is obtained through higher polynomial order fits. We then turned back to configurations R, U, V and found that a cubic fit of the $\langle\kappa\rangle_l$ values such that $Rm < Rm^*$ provides an extrapolated threshold value Rm^e that is close to the Rm^* determined via real data. We thus run this cubic extrapolation technique to Q', S, and T and obtain values of Rm^e that are reported in the table. The extrapolated values found here are generally smaller than the one found by Miralles *et al* [12], but in both cases the extrapolation presents great uncertainty.

In this article, we have tested a methodology for the detection of the dynamo threshold based on EVT, using datasets produced in the VKS experiment. This technique, applied here for the first time to an experimental dataset, confirms the theoretical expectations of [14] and allows for detecting hysteretic behaviors. The main advantage of the technique is to provide a precise and unambiguous estimate of the thresholds on a probabilistic basis, providing the direction of the shift (towards the *maxima* or the *minima*). The analysis is affordable with every home PC,

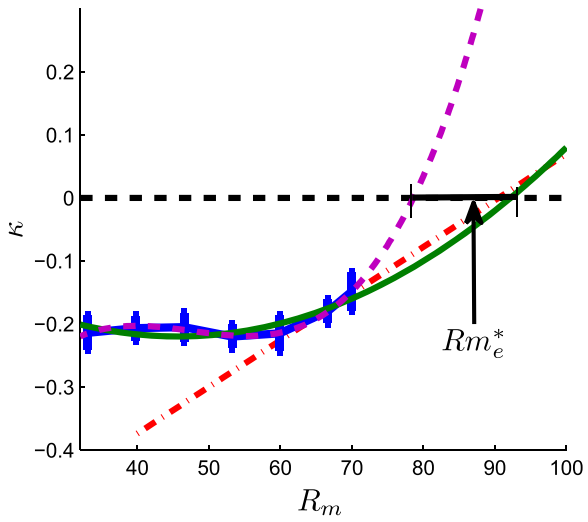

Figure 8. Diagram of $\langle \kappa \rangle_l$ (blue solid error bar) and Gumbel law $\kappa = 0$ (dashed black line) in the Q' configuration versus magnetic Reynolds number. The red dashed-dotted line, the green solid line, and the magenta dashed line represent respectively the linear, quadratic, and cubic fits of the data. The linear fit is obtained by considering only the three values of $\langle \kappa \rangle_l$ at higher Rm, $m = 4000$.

and many software packages contain the routine necessary for performing the fit of the GEV distribution. In light of the possibility of extracting the magnetic field data from exoplanetary radio emissions, one could exploit the technique described in this article for studying the properties of exoplanetary magnetospheres, thus defining a criterion for the classification of planetary dynamos based on the detected threshold values. Moreover, since hysteretic behaviours are encountered in many other scientific fields, e.g., thermohaline circulation reversibility [28] in climate sciences or economical crisis behavior [29], we consider the method to be applicable to a more general class of problems featuring critical transitions.

Acknowledgments

We thank the other members of the VKS collaboration with whom the experimental runs have been performed. We thank M Moulin, C Gasquet, A Skiara, N Bonnefoy, D Courtiade, J-F Point, P Metz, V Padilla, and M Tanase for their technical assistance. This work is supported by ANR 08-0039-02, Direction des Sciences de la Matière, and Direction de l'Energie Nucléaire of CEA, Ministère de la Recherche, and CNRS. The experiment is operated at CEA/Cadarache DEN/DTN.

References

[1] Stieglitz R and Müller U 2001 *Phys. Fluids* **13** 561
[2] Rädler K-H, Apstein E, Rheinhardt M and Schüler M 1998 *Studia geophysica et geodaetica* **42** 224
[3] Gailitis A, Lielausis O, Platacis E, Dement'ev S, Cifersons A, Gerbeth G, Gundrum T, Stefani F, Christen M and Will G 2001 *Phys. Rev. Lett.* **86** 3024

[4] Leprovost N and Dubrulle B 2005 *The European Physical Journal B-Condensed Matter and Complex Systems* **44** 395
[5] Berhanu M *et al* 2007 *EPL (Europhysics Letters)* **77** 59001
[6] Spence E, Nornberg M, Jacobson C, Parada C, Taylor N, Kendrick R and Forest C 2007 *Phys. rev. lett.* **98** 164503
[7] Kelley D H, Triana S A, Zimmerman D S, Tilgner A and Lathrop D P 2007 *Geophys. Astrophys. Fluid Dyn.* **101** 469
[8] Scheffer M, Bascompte J, Brock W A, Brovkin V, Carpenter S R, Dakos V, Held H, van Nes E H, Rietkerk M and Sugihara G 2009 *Nature* **461** 53
[9] Kuehn C 2011 *Physica* D **240** 1020
[10] Monchaux R *et al* 2009 *Phys. Fluids* **21** 035108
[11] Berhanu M *et al* 2009 *J. Fluid Mech.* **641** 217
[12] Miralles S, Bonnefoy N, Bourgoin M, Odier J-F P, Nicolas P, Verhille G, Boisson J, Daviaud F and Dubrulle B 2013 *Phys. Rev.* E **88** 013002
[13] Lahjomri J, Capéran P and Alemany A 1993 *J. Fluid Mech.* **253** 421
[14] Faranda D, Lucarini V, Manneville P and Wouters J 2014 *Chaos Solitons Fractals* **64** 26–35
[15] Boisson J, Aumaitre S, Bonnefoy N, Bourgoin M, Daviaud F, Dubrulle B, Odier P, Pinton J, Plihon N and Verhille G 2012 *New J. Phys.* **14** 013044
[16] Miralles S *et al* 2014 *Phys. Rev.* E **89** 063023
[17] Gallet B *et al* 2012 *Phys. Rev. Lett.* **108** 144501
[18] Leadbetter M R, Lindgren G and Rootzén H 1983 *Extremes and Related Properties of Random Sequences and Processes* Springer Series in Statistics (New York: Springer-Verlag) p xii+336
[19] Coles S, Bawa J, Trenner L and Dorazio P 2001 *An Introduction to Statistical Modeling of Extreme Values* (London: Springer)
[20] Holland M P, Vitolo R, Rabassa P, Sterk A E and Broer H W 2012 *Physica* D **241** 497
[21] Lucarini V, Faranda D, Turchetti G and Vaienti S 2012 *Chaos* **22** 023135
[22] Hall P 1979 *J. Appl. Probab.* **16** 433–9
[23] Faranda D, Lucarini V, Turchetti G and Vaienti S 2012 *Int. J. Bifurcat. Chaos* **22** 1250276
[24] Bourgoin M *et al* 2002 *Phys. Fluids* **14** 3046
[25] Eckmann J-P and Ruelle D 1992 *Physica D: Nonlinear Phenomena* **56** 185
[26] Faranda D, Lucarini V, Turchetti G and Vaienti S 2011 *J. Stat. Phys* **145** 1156
[27] Berhanu M *et al* 2010 *Eur. Phys. J.* B **77** 459
[28] Rahmstorf S *et al* 2005 *Geophy. Res. Lett.* **32** L23605
[29] Martin R 2012 *J. Econ. Geogr.* **12** 1